

See discussions, stats, and author profiles for this publication at: <https://www.researchgate.net/publication/341069214>

Adaptive Robust Kernels for Non-Linear Least Squares Problems

Preprint · April 2020

CITATIONS

0

READS

108

5 authors, including:



Nived Chebrolu

University of Bonn

14 PUBLICATIONS 115 CITATIONS

[SEE PROFILE](#)



Thomas Läbe

University of Bonn

31 PUBLICATIONS 370 CITATIONS

[SEE PROFILE](#)



Olga Vysotska

University of Bonn

15 PUBLICATIONS 174 CITATIONS

[SEE PROFILE](#)

Some of the authors of this publication are also working on these related projects:



EUROPA2 [View project](#)



PhenoRob – Robotics and Phenotyping for Sustainable Crop Production [View project](#)

Adaptive Robust Kernels for Non-Linear Least Squares Problems

Nived Chebrolu

Thomas Läbe

Olga Vysotska

Jens Behley

Cyrill Stachniss

Abstract—State estimation is a key ingredient in most robotic systems. Often, state estimation is performed using some form of least squares minimization. Basically, all error minimization procedures that work on real-world data use robust kernels as the standard way for dealing with outliers in the data. These kernels, however, are often hand-picked, sometimes in different combinations, and their parameters need to be tuned manually for a particular problem. In this paper, we propose the use of a generalized robust kernel family, which is automatically tuned based on the distribution of the residuals and includes the common m-estimators. We tested our adaptive kernel with two popular estimation problems in robotics, namely ICP and bundle adjustment. The experiments presented in this paper suggest that our approach provides higher robustness while avoiding a manual tuning of the kernel parameters.

I. INTRODUCTION

State estimation is a central building block in robotics and is used in a variety of different components, such as simultaneous localization and mapping (SLAM). A large number of state estimation solvers perform some form of non-linear least squares minimization. Prominent examples are the optimization of SLAM graphs, the ICP algorithm, visual odometry, or bundle adjustment (BA), which all seek to find the minimum of some error function. As soon as real-world data is involved, outliers will occur in the data. A common source of such outliers stems from data association mistakes, for example, when matching features.

To avoid that even a few such outliers have strong effects on the final solution, robust kernel functions are used to down-weight the effect of gross errors. Several robust kernels have been developed to deal with outliers arising in different situations. Prominent examples include the Huber, Cauchy, Geman-McClure, or Welsh functions that can be used to obtain a robustified estimator [23].

However, the proper choice of the best kernel for a given problem is not straightforward. As the robust kernels define the distribution from which the outliers are generated, their choice is problem-specific. In practice, the choice of the kernel is often done in a trial and error manner, as in most situations there is no prior knowledge of the outlier process. For some approaches such as bundle adjustment, today's implementations even vary the kernel between iterations or pair them with outlier rejection heuristics. Moreover, for several robotics applications such as SLAM, the outlier distribution itself changes continuously depending on the structure of the environment, dynamic objects in the scene

All authors are with the University of Bonn, Germany. O. Vysotska is also with the Autonomous Intelligent Driving GmbH, Munich, Germany.

This work has partially been funded by the Deutsche Forschungsgemeinschaft (DFG, German Research Foundation) under Germany's Excellence Strategy, EXC-2070 - 390732324 - PhenoRob.

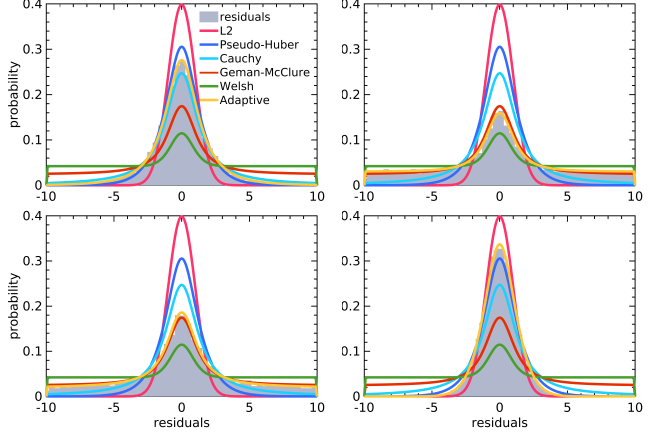


Fig. 1. Probability densities of different robust kernels. The adaptive robust kernel (in yellow) is able to describe the actual residual distribution in different situations better than a fixed robust kernel for all cases. As a result, it provides better robustness to different types of outliers during the state estimation process.

and other environmental factors like lighting. This often means that a fixed robust kernel chosen a-priori cannot deal effectively with all situations.

In this paper, we aim at circumventing the trial and error process for choosing a kernel and at exploring the automatic adaptation of kernels to the outliers online. To achieve this, we use a family of robust loss functions proposed by Barron [5], which generalizes several popular robust kernels such as Huber, Cauchy, Geman-McClure, Welsh, etc. The key idea is to dynamically tune this generalized loss function automatically based on the current residual distribution so that one can blend between such robust kernels and make the choice a part of the optimization problems.

The main contribution of this paper is an easy-to-implement approach for dynamically adapting the robust kernels in non-linear least squares (NLS) solvers based on the generalized formulation of Barron [5]. We achieve this by estimating a hyper-parameter for a generalized loss function, which controls the shape of the robust kernel. This parameter becomes part of the estimation process in an expectation-maximization fashion. This allows us to better deal with different outlier distributions compared to a fixed kernel. See Fig. 1 for a visualization.

In sum, we make the following key claims. Our approach can (i) perform robust estimation without committing to a fixed kernel beforehand, (ii) adapt the shape of the kernel to the actual outlier distribution, and (iii) illustrate the performance on two common example problems, namely ICP and bundle adjustment.

II. RELATED WORK

Robust kernels are the de-facto solution to perform state estimation using least-squares minimization in the presence of outliers. To deal with different outlier distributions, several robust kernels such as Huber, Cauchy, Geman-McClure, or Welsh have been proposed in the literature [7], [23]. Babin *et al.* [4] provide an analysis of popular robust kernels for registration problems and advice for using different kernels depending on the scenario. Similar analysis and recommendations exists for visual odometry and BA in [16], [22].

In this work, instead of choosing a specific robust kernel for a particular scenario, we dynamically adapt a robust kernel to the actual outlier distribution during the optimization process. To do this, we build upon the generalized kernel formulation recently proposed by Barron [5] for training neural networks. It generalizes over popular robust kernels and we formulate an approximation of it for the use in NLS estimation.

For pose graph SLAM problems, several approaches exist to deal with the outliers dynamically. Sünderhauf and Protzel [19] propose introducing additional switch variables to the original optimization problem, which determines whether an observation should be used or discarded during optimization. Agarwal *et al.* [2] propose a robust kernel, which dynamically weighs the observations without requiring to estimate any additional variables. Lajoie *et al.* [15] and Yang *et al.* [21] further this idea as a truncated least squares problem which can be solved efficiently as a semi-definite program. They also provide solutions with certain robustness guarantees for the registration and SLAM problem. Recently, Yang *et al.* [20] propose a robust estimation framework based on graduated non-convexity (GNC) methods which solves a sequence of minimization problems which are convex initially, and converge eventually to the original non-convex robust loss.

Taking a probabilistic view, several robust kernels are understood to arise from a probability distribution, which can be used to determine the best kernel type based on the actual observations. Agamennoni *et al.* [1] propose to use an elliptical distribution to represent several popular robust kernels. They estimate hyper-parameters for each kernel type based on the residual distribution and perform a model comparison to determine the best kernel for the situation at hand. In this paper, we take a different approach and adapt the robust kernel shape by using the probability distribution of a generalized loss function [5]. We do not require an explicit model comparison to choose the best kernel and estimate the kernel shape in an EM fashion with the optimizations.

III. LEAST SQUARES WITH AN ADAPTING KERNEL

Our approach targets dynamically adapting robust kernels when solving NLS problems by estimating a hyper-parameter that controls the shape of the robust kernel. This parameter becomes part of the estimation process in an expectation-maximization fashion. Before explaining our approach, we

first explain robust NLS estimation and generalized kernels to give the reader a complete view.

A. Robust Least Squares Estimation

Several state estimation problems in robotics involve estimating unknown parameters θ of a model given noisy observations z_i with $i = 1, \dots, N$. These problems are often framed as non-linear least squares optimization, which aims to minimize the squared loss:

$$\theta^* = \underset{\theta}{\operatorname{argmin}} \frac{1}{2} \sum_{i=1}^N w_i \|r_i(\theta)\|^2, \quad (1)$$

where $r_i(\theta) = f_i(\theta) - z_i$ is the residual and w_i is the weight for the i^{th} observation. The estimate θ^* is statistically optimal if the error on the observations z_i is Gaussian. In case of non-Gaussian noise, however, the estimate θ^* can be arbitrarily poor [11]. To reduce this impact of outliers, sub-quadratic losses can be applied. The main idea of a robust loss is to downweight large residuals that are assumed to be caused from outliers such that their influence on the solution is reduced. This is achieved by optimizing:

$$\theta^* = \underset{\theta}{\operatorname{argmin}} \sum_{i=1}^N \rho(r_i(\theta)), \quad (2)$$

where $\rho(r)$ is also called the robust loss or kernel. Several robust kernels have been proposed to deal with different kinds of outliers such as Huber, Cauchy, and others [23].

The optimization problem in Eq. (2) can be solved using the iteratively reweighted least squares (IRLS) approach [23], which solves a sequence of weighted least squares problems. We can see the relation between the least squares optimization in Eq. (1) and robust loss optimization in Eq. (2) by comparing the respective gradients which go to zero at the optimum (illustrated only for the i^{th} residual):

$$\frac{1}{2} \frac{\partial(w_i r_i^2(\theta))}{\partial \theta} = w_i r_i(\theta) \frac{\partial r_i(\theta)}{\partial \theta} \quad (3)$$

$$\frac{\partial(\rho(r_i(\theta)))}{\partial \theta} = \rho'(r_i(\theta)) \frac{\partial r_i(\theta)}{\partial \theta}. \quad (4)$$

By setting the weight $w_i = \frac{1}{r_i(\theta)} \rho'(r_i(\theta))$, we can solve the robust loss optimization problem by using the existing techniques for weighted least-squares. This scheme allows standard solvers using Gauss-Newton and Levenberg-Marquardt algorithms to optimize for robust losses and is implemented in popular optimization frameworks such as Ceres [3], g2o [13], and iSAM [12].

B. Adaptive Robust Kernel

Barron [5] proposes a single robust kernel that generalizes for several popular kernels such as pseudo-Huber/L1-L2, Cauchy, Geman-McClure, Welsh. The generalized kernel ρ is given by:

$$\rho(r, \alpha, c) = \frac{|\alpha - 2|}{\alpha} \left(\left(\frac{(r/c)^2}{|\alpha - 2|} + 1 \right)^{\alpha/2} - 1 \right), \quad (5)$$

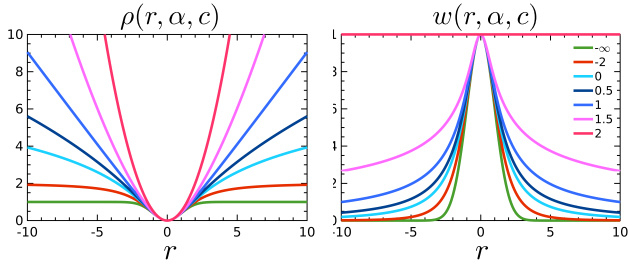


Fig. 2. Left: General robust loss $\rho(r, \alpha, c)$ takes different shapes depending on the value of α . Right: Corresponding weights for kernels with different α values. A smaller α corresponds to a larger down-weighting of the residuals.

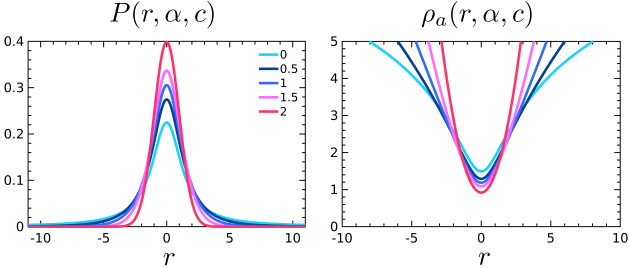


Fig. 3. Left: Probability distribution $P(r, \alpha, c)$ of generalized robust loss function for different values of α . Right: Adaptive robust loss $\rho_a(r, \alpha, c)$ obtained as the negative log-likelihood of $P(r, \alpha, c)$. This adaptive loss enables automatic tuning of $\alpha \in [0, 2]$.

where α is a real-valued parameter that controls the shape of the kernel and $c > 0$ is the scale parameter that determines the size of quadratic loss region around $r = 0$. Adjusting the parameter α essentially allows us to realize different robust kernels. Some special cases are squared/L2 loss ($\alpha = 2$), pseudo-Huber/L1-L2 ($\alpha = 1$), Cauchy ($\alpha = 0$), Geman-McClure ($\alpha = -2$), and Welsh ($\alpha = -\infty$).

The general loss function $\rho(r, \alpha, c)$ and the corresponding weights curve $w(r, \alpha, c)$ are illustrated in Fig. 2 for several values of α . The shape of the weights curve provides an insight into the influence that a residual has on the solution while minimizing the robust loss function in Eq. (2). For example, for $\alpha = 2$, the weights for all residuals are one, meaning that all residuals are treated the same. Whereas for $\alpha = -\infty$, all residuals greater than $3c$ will not affect the solution θ^* as they are weighed down completely.

With this generalized robust loss, we can interpolate between a range of robust kernels simply by tuning α . To automatically determine the best kernel shape through the parameter α , we treat α as an additional unknown parameter while minimizing the generalized loss:

$$(\theta^*, \alpha^*) = \underset{(\theta, \alpha)}{\operatorname{argmin}} \sum_{i=1}^N \rho(r_i(\theta), \alpha). \quad (6)$$

However, this optimization problem in Eq. (6) can be trivially minimized by choosing an α that weighs down all residuals to zero without affecting the model parameters θ , essentially treating all data points as outliers. Barron [5] avoids this situation by constructing a probability distribution

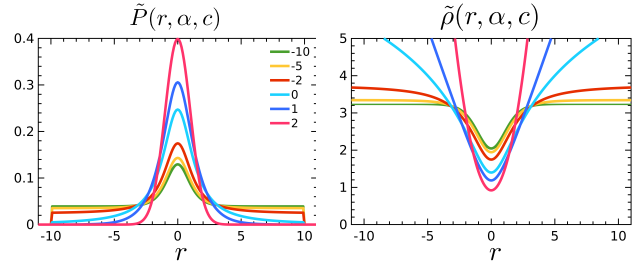


Fig. 4. Left: Modified probability distribution $\tilde{P}(r, \alpha, c)$ obtained by truncating $P(r, \alpha, c)$ at $|r| < \tau$. Right: The truncated robust loss $\tilde{\rho}_a(r, \alpha, c)$ allows the automatic tuning of α in its complete range, including $\alpha < 0$.

based on the generalized loss function $\rho(r, \alpha, c)$ as

$$P(r, \alpha, c) = \frac{1}{cZ(\alpha)} e^{-\rho(r, \alpha, c)} \quad (7)$$

$$Z(\alpha) = \int_{-\infty}^{\infty} e^{-\rho(r, \alpha, 1)} dr, \quad (8)$$

where $Z(\alpha)$ is a normalization term, also called partition function, which defines an adaptive general loss as the negative log-likelihood of Eq. (7),

$$\rho_a(r, \alpha, c) = -\log P(r, \alpha, c) \quad (9)$$

$$= \rho(r, \alpha, c) + \log cZ(\alpha). \quad (10)$$

The adaptive loss $\rho_a(\cdot)$ is simply the general loss $\rho(\cdot)$ shifted by the log partition. This shift introduces an interesting trade-off. A lower cost for increasing the set of outliers comes with a penalty for the inliers and vice versa. This trade-off forces the optimization in Eq. (6) to choose a suitable value for α instead of trivially ignoring all residuals by turning every data point into an outlier. The probability distribution $P(r, \alpha, c)$ and the adaptive loss function are plotted in Fig. 3 for visualization.

C. Truncated Robust Kernel

The probability distribution $P(r, \alpha, c)$ is only defined for $\alpha \geq 0$, as the integral in the partition function $Z(\alpha)$ is unbounded for $\alpha < 0$. This means that values for $\alpha < 0$ cannot be achieved while minimizing the adaptive loss $\rho_a(\cdot)$ in Eq. (9). This limits the range of kernels that we can dynamically adapt to. As we can see in Fig. 2, the smaller the parameter α is, the stronger is the down-weighting of outliers. Such a behavior is often desired in situations where a large number of outliers are present in the data.

We propose to limit the partition to bounded values. To re-gain the kernels corresponding to the negative range of α with the adaptive loss function, we compute an approximate partition function $\tilde{Z}(\alpha)$ as

$$\tilde{Z}(\alpha) = \int_{-\tau}^{\tau} e^{-\rho(r, \alpha, 1)} dr, \quad (11)$$

where τ is the truncation limit for approximating the integral. This results in a finite partition $\tilde{Z}(\alpha)$ for all α as the integral

Algorithm 1 Optimization with adaptive robust kernel

- 1: Initialize $\theta^0 = \theta, \alpha^0 = 2, c$
- 2: **while** !converged **do**
- 3: E-step: 1-D grid search
- 4: $\alpha^t = \operatorname{argmax}_\alpha \sum_{i=1}^N \log P(r_i(\theta^{t-1}), \alpha^{t-1}, c)$
- 5: M-step: Minimize robust loss using IRLS
- 6: $\theta^t = \operatorname{argmin}_\theta \sum_{i=1}^N \rho(r_i(\theta), \alpha^t, c),$

is computed within the limits $[-\tau, \tau]$. We use this to define our truncated loss function as

$$\tilde{\rho}_a(r, \alpha, c) = \rho(r, \alpha, c) + \log c\tilde{Z}(\alpha). \quad (12)$$

The truncated probability distribution $\tilde{P}(r, \alpha, c)$ and the corresponding truncated loss $\tilde{\rho}_a(r, \alpha, c)$ is shown in Fig. 4. Since the truncated loss is defined for all values of α including $\alpha < 0$, we can adapt α in its entire range during the optimization procedure. We discuss the effect of the truncation of the loss function below in Sec. III-E.

D. Optimization of α via Expectation-Maximization

We propose to solve the joint optimization problem over θ and α , see Eq. (6), in an iterative manner using an expectation-maximization (EM) procedure. An EM procedure alternates between two steps: (i) the expectation (E) step where the maximum likelihood value for the latent variables are computed, and (ii) the maximization (M) step, where the optimal parameters of the model given the latent variables from the E-step are computed. By solving the joint optimization in this manner, we decouple the estimation of the robust kernel parameter α from the original optimization problem. This allows to us solve for the model parameters θ in the same way as before α was introduced.

In our case, the E-step computes the maximum likelihood estimate of α given the residual distribution for the current estimate θ . The M-step involves minimizing the robust loss using the α value computed in the previous E-step. We estimate α in the E-step by maximizing the log-likelihood of observing the current residuals,

$$L(\alpha) = \sum_{i=1}^N \log P(r_i(\theta), \alpha, c) \quad (13)$$

$$= - \sum_{i=1}^N \log c\tilde{Z}(\alpha) + \rho_a(r_i(\theta), \alpha, c), \quad (14)$$

$$\text{i.e., } \alpha^* = \operatorname{argmax}_\alpha L(\alpha). \quad (15)$$

The solution to Eq. (15) can be obtained by setting its first derivative $\frac{dL(\alpha)}{d\alpha} = 0$. Since its not possible to derive the partition function $\tilde{Z}(\alpha)$ analytically, we settle for a numerical solution. As α is a scalar value, $L(\alpha)$ can be maximized simply by performing a 1-D grid search for $\alpha \in [\alpha_{min}, 2]$.

In terms of implementation, we chose lower bound $\alpha_{min} = -10$ as its difference to the corresponding weights for $\alpha = -\infty$ for large residuals ($|r| > \tau$) is small. The maximum value for α is set to 2 as this corresponds to the standard least squares problem. The scale c of the

robust loss is fixed beforehand and not adapted during the optimization. This value for c is usually fixed based on the measurement noise for an inlier observation z and the accuracy of the initial solution. To be computationally efficient, we pre-compute the $\tilde{Z}(\alpha)$ as a lookup table for $\alpha \in [\alpha_{min}, 2]$ with a resolution of 0.1 and use the lookup table during optimization. This leads us to the overall minimization approach as shown in Alg. 1.

E. Effect of Using the Truncated Loss

The M-Step, i.e. the *minimization* in the NLS estimation, is not affected by the truncated loss approximation. It can, however, affect the E-Step, i.e. determining α . By using our truncated loss, we are implicitly assuming that no outliers have a residual $|r| > \tau$ during the E-Step. If we choose a large enough τ , the error that we introduce affects situations with large outliers only and therefore resulting in small α values. The effect of small α values such as $\alpha = -10$ vs. $\alpha = -\infty$ on the optimization, however, is negligible as the outliers will be down-weighted to zero. Thus, on our experiments, we choose $\tau = 10c$ as this covers almost all of the observations in the practical applications related to ICP, SLAM, BA, etc.

IV. EXPERIMENTAL EVALUATION

A. Application to Iterative Closest Point

The first experiment is designed to show the advantages of our approach for LiDAR-based registration in form of ICP. We integrated our truncated adaptive robust kernel to the existing SLAM system, called surfel-based mapping (SuMa) [6], which performs point-to-plane projective ICP for 3D LiDAR scans. First, we compare the performance of our approach against a fixed robust kernel used in SuMa, i.e. Huber. Second, we compare it to the Huber kernel plus an additional, hand-crafted outlier rejection step before optimization as used in the original implementation [6]. This outlier rejection step removes all correspondences, which have a distance of more than 2 m or which have an angular difference greater than 30° between the estimated normals of observations and the corresponding normals of the surfels.

We evaluate all three approaches on the odometry datasets of the KITTI Vision Benchmark [10] and summarize the results in Tab. I. We observe that our proposed approach, which does *not* require an outlier rejection step at all, performs better or is on-par with fixed kernel plus outlier rejection scheme for all the sequences. At the same time, using only the fixed kernel without the outlier rejection step fails for several sequences. These results are promising as by using our adaptive robust kernel, we do not need any hand-crafted outlier rejection mechanism, which in practice requires manual tuning for new data or different sensor configurations.

We illustrate the advantage of using the adaptive robust kernel for a challenging dataset (Seq. 01, “KITTI highway sequence”), which contains several moving cars moving with the vehicle itself along the highway with little additional geometric structures. In Fig. 5 (top-left), we plot the values of

TABLE I
RESULTS ON KITTI ODOMETRY DATASETS [RELATIVE ROT. ERROR IN degrees PER 100 M / RELATIVE TRANS. ERROR IN %]

Approach	Sequence											Average
	00	01	02	03	04	05	06	07	08	09	10	
Our Approach	1.5/2.8	1.3/3.8	0.91/1.8	1.5/1.9	0.81/0.95	0.97/1.7	0.51/1.1	2.1/2.6	1.3/2.7	0.8/1.4	1.3/1.7	1.18/2.03
Fixed Kernel	0.93/2.1	1.2/4.5	0.79/2.3	0.7/1.4	1.1/49	0.79/1.5	0.64/0.95	1.2/1.8	0.96/2.5	0.78/1.9	0.97/1.8	0.92/6.34
Fixed Kernel with Outlier Rejection [6]	0.9/2.1	1.2/4.0	0.8/2.3	0.7/1.4	1.1/11.9	0.8/1.5	0.6/1.0	1.2/1.8	1.0/2.5	0.8/1.9	1.0/1.8	0.9/2.9

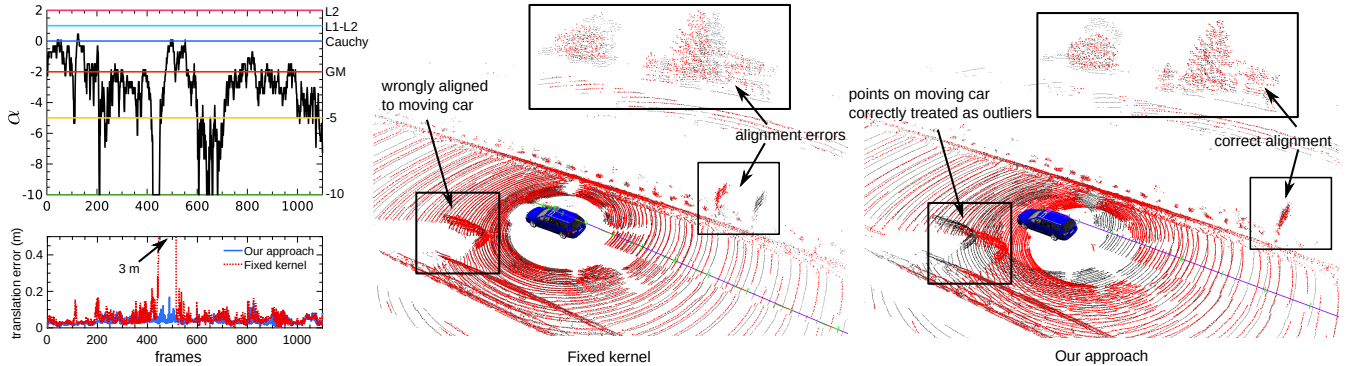


Fig. 5. Our approach on a challenging dataset for ICP. Top-left: Plot showing α values estimated at each frame based on the residual distribution for KITTI 01 sequence. Bottom-Left: Translation error (in meters) for our approach and fixed kernel ICP. We observe lower α values (stronger outlier down-weighting) for scan matches with outliers arising from dynamic objects in the scene. Middle-right: ICP result from an example frame where ICP converges for adaptive kernel whereas it diverges for a fixed kernel.

α for each iteration while mapping the sequence. We observe that α adapts to smaller and more negative values whenever there are more outliers, which arise mainly from moving vehicles in the scan. This effect can be seen in Fig. 5 (bottom-left) where the translation error for the fixed kernel increases as it cannot handle the outlier situation well. At the same time, the error remains small for our adaptive kernel.

The two 3D scenes show the registrations at the same point in time, once computed with the adaptive kernel and once with a fixed one. The adaptive kernel results in a successful alignment while the fixed kernel fails to find the correct solution due to the outlier in the data association, see Fig. 5 (middle and right). The adaptive kernel-based ICP can correctly treat the observations belonging to the moving car as outliers, and nullify their effect during optimization automatically. For this sequence, we note that for large portions of the scans, α is negative and even reaches down to $\alpha_{\min} = -10$ in some instances. This suggests that our truncated adaptive loss proposed in Eq. (12) is critical for the successful application of ICP as it enables using values $\alpha < 0$, whereas the original formulation of the adaptive loss is limited to $\alpha \in [0, 2]$. Thus, our approach greatly supports ICP-based registration as it avoids hand-crafted outlier strategies and adapts to the outlier challenges present in each pairs of scans automatically.

B. Application to Bundle Adjustment (BA)

The second experiment is designed to illustrate the performance of our approach and its advantages for the bundle adjustment problem using a monocular camera. We integrated the adaptive robust kernel to an existing bundle adjustment framework proposed by Schneider *et al.* [18].



Fig. 6. Examples images from CARLA dataset. Left: image from a front-looking camera mounted on a car. Right: side facing image.

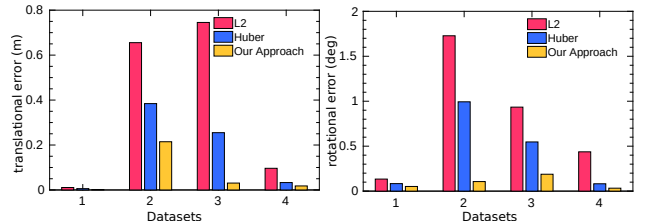


Fig. 7. Translation and rotational errors for BA on different datasets.

The initial estimate for camera poses and 3D points is obtained by three commonly used steps. First, extract SIFT features and compute possible matches between all image pairs. Second, compute the relative orientation using Nister's 5-point algorithm [17] together with RANSAC for outlier rejection and chaining the subsequent images to obtain the initial camera trajectory. Third, compute the 3D points as described in [14] given the camera trajectory of the second step.

To test the bundle adjustment performance, we created four datasets covering different scenarios using the CARLA simulator [9] generating near-realistic images. The advantage of the simulator is that ground truth information for the

cameras poses is available. The first dataset contains images from a front looking camera mounted on a car, the second dataset simulates downward looking aerial images from a UAV, the third dataset contains images where around half of each image shows strong shadows, and the fourth dataset simulates side-ward looking camera where close-by objects suffer from significant motion blur. Two example images from the dataset 1 and 3 are depicted in Fig. 6.

For each of these datasets, we evaluate the bundle adjustment results by comparing the performance of our approach against squared error loss as well as the standard Huber loss as a fixed kernel. We compute the accuracy of the camera pose estimates by comparing against the ground truth poses from the simulator as described in [8]. Fig. 7 illustrates the results for all the four datasets where our approach has a lower translation and rotational error than using squared error or the fixed Huber kernel. We obtain a translation and rotational error, which is between 2 to 5 times better as compared to using Huber depending on the dataset. We perform the ground truth comparison only based on the camera poses and do not consider the 3D point as they have been extracted using the SIFT descriptor from the simulated images and thus no ground truth 3D information is available.

The last experiment is designed to analyze the influence of our approach on the convergence properties of BA. A large basin of convergence is important for robust operation, especially for BA due to the missing range information with the image data. We initialized the bundle adjustment procedure by adding significant noise to the initial camera poses, i.e. $\sigma \in [0.1 \text{ m}, 5 \text{ m}]$ to the ground truth poses of the camera. The noise in the camera poses is propagated to the 3D points during the forward intersection step. We sample 20 instances of each noise level (500 instances in total) and run the bundle adjustment for our approach, using squared loss, the Geman-McClure as well as the Huber kernel. We consider the adjustment to have converged if the final RMS error of the camera center is less than 1 cm from the true position. We visualize the results in Fig. 8 where the poses from which the BA has converged are shown in green and the ones that caused divergence in red. We can clearly see that our approach has a larger convergence radius as the green points are spread over a larger area compared to the squared loss or fixed Huber or Geman-McClure kernel. We obtain successful convergence rate for 45% of all instances for our approach against 24.8% for squared loss, 33% for Huber, and 28.2% for Geman-McClure. Overall, the experiments suggest that by using our approach, we can obtain a more accurate estimate and have a larger convergence area as compared to a fixed kernel. Thus, our approach is an effective and useful approach for optimization in bundle adjustment problems.

V. CONCLUSION

In this paper, we presented a novel approach to robust optimization that avoids the need to commit to a fixed robust kernel and potentially has a broad application area for state estimation in robotics. We proposed the use of a generalized robust kernel that can adapt its shape with an additional

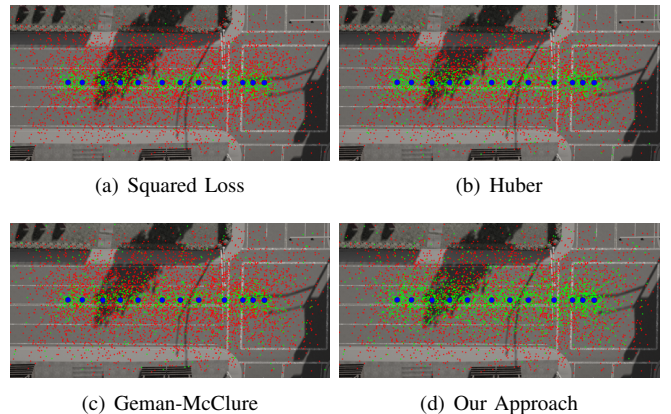


Fig. 8. Convergence analysis for BA. Green points indicate poses for which BA converged, whereas red points indicate divergence. The blue circles represent the ground truth camera poses.

parameter that has recently been proposed by Barron [5]. We modified the original formulation, which enables us to use the adaptive kernel also in situations with strong outliers. We integrated our adaptive kernel into and tested it for two popular state estimation problems in robotics, namely ICP and bundle adjustment. The experiments showcase that we are better or on-par with fixed kernels such as Huber or Geman-McClure but do not require hand-crafted outlier rejection schemes in the case of ICP and can increase the radius of convergence for bundle adjustment. We believe that several other problems in robotics, which rely on robust least-squares estimation, can benefit from our proposed approach.

REFERENCES

- [1] G. Agamennoni, P.T. Furgale, and R. Siegwart. Self-Tuning M-Estimators. In *Proc. of the IEEE Intl. Conf. on Robotics & Automation (ICRA)*, 2015.
- [2] P. Agarwal, G.D. Tipaldi, L. Spinello, C. Stachniss, and W. Burgard. Robust Map Optimization using Dynamic Covariance Scaling. In *Proc. of the IEEE Intl. Conf. on Robotics & Automation (ICRA)*, 2013.
- [3] S. Agarwal, K. Mierle, and Others. Ceres Solver. <http://ceres-solver.org>, 2010.
- [4] P. Babin, P. Giguere, and F. Pomerleau. Analysis of robust functions for registration algorithms. In *Proc. of the IEEE Intl. Conf. on Robotics & Automation (ICRA)*, 2019.
- [5] J. T. Barron. A General and Adaptive Robust Loss Function. In *Proc. of the IEEE Conf. on Computer Vision and Pattern Recognition (CVPR)*, 2019.
- [6] J. Behley and C. Stachniss. Efficient Surfel-Based SLAM using 3D Laser Range Data in Urban Environments. In *Proc. of Robotics: Science and Systems (RSS)*, 2018.
- [7] M. Bosse, G. Agamennoni, and I. Gilitschenski. Robust estimation and applications in robotics. *Foundations and Trends in Robotics*, 4(4):225–269, 2016.
- [8] T. Dickscheid, T. Läbe, and W. Förstner. Benchmarking automatic bundle adjustment results. In *Cong. of the Intl. Society for Photogrammetry and Remote Sensing (ISPRS)*, 2008.
- [9] A. Dosovitskiy, G. Ros, F. Codevilla, A. Lopez, and V. Koltun. CARLA: An open urban driving simulator. In *Proc. of the Conf. on Robot Learning*, 2017.
- [10] A. Geiger, P. Lenz, and R. Urtasun. Are we ready for Autonomous Driving? The KITTI Vision Benchmark Suite. In *Proc. of the IEEE Conf. on Computer Vision and Pattern Recognition (CVPR)*, 2012.
- [11] P. J. Huber. Robust estimation of a location parameter. *Annals of Mathematical Statistics*, 35(1):73–101, 1964.
- [12] M. Kaess, A. Ranganathan, and F. Dellaert. iSAM: Incremental smoothing and mapping. *IEEE Trans. on Robotics (TRO)*, 24(6), 2008.
- [13] R. Kümmerle, G. Grisetti, H. Strasdat, K. Konolige, and W. Burgard. g2o: A general framework for graph optimization. In *Proc. of the IEEE Intl. Conf. on Robotics & Automation (ICRA)*, pages 3607–3613, 2011.

- [14] T. Läbe and W. Förstner. Automatic relative orientation of images. In *Proc. of the Turkish-German Joint Geodetic Days*, 2006.
- [15] P. Lajoie, S. Hu, G. Beltrame, and L. Carlone. Modeling perceptual aliasing in SLAM via discrete-continuous graphical models. *IEEE Robotics and Automation Letters (RA-L)*, 2019.
- [16] K. MacTavish and T. D. Barfoot. At all costs: A comparison of robust cost functions for camera correspondence outliers. In *Proc. of the Conf. on Computer and Robot Vision*, pages 62–69, 2015.
- [17] D. Nistér. An efficient solution to the five-point relative pose problem. *IEEE Trans. on Pattern Analysis and Machine Intelligence (TPAMI)*, 26(6):756–770, 2004.
- [18] J. Schneider, F. Schindler, T. Läbe, and W. Förstner. Bundle adjustment for multi-camera systems with points at infinity. In *ISPRS Annals of Photogrammetry, Rem. Sens. and Spatial Inf. Sci.*, volume I-3, 2012.
- [19] N. Sünderhauf and P. Protzel. Switchable constraints for robust pose graph slam. In *Proc. of the IEEE/RSJ Intl. Conf. on Intelligent Robots and Systems (IROS)*, pages 1879–1884, 2012.
- [20] H. Yang, P. Antonante, V. Tzoumas, and L. Carlone. Graduated non-convexity for robust spatial perception: From non-minimal solvers to global outlier rejection. *IEEE Robotics and Automation Letters (RA-L)*, 5(2):1127–1134, 2020.
- [21] H. Yang, J. Shi, and L. Carlone. TEASER: Fast and Certifiable Point Cloud Registration. *arXiv preprint arXiv: 2001.07715*, 2020.
- [22] C. Zach. Robust bundle adjustment revisited. In *Proc. of the Europ. Conf. on Computer Vision (ECCV)*, pages 772–787, 2014.
- [23] Z. Zhang. Parameter estimation techniques: A tutorial with application to conic fitting. *Image and Vision Computing*, 15:59–76, 1997.